PRAMANA
— journal of
physics

Vol. 76, No. 6
June 2011
pp. 909–919

Stability of the fragments and thermalization at the peak centre-of-mass energy

AMAN D SOOD[1,*] and SUKHJIT KAUR[2]

[1]SUBATECH, Laboratoire de Physique Subatomique et des Technologies Associées, Université de Nantes-IN2P3/CNRS-EMN, 4 rue Alfred Kastler, F-44072 Nantes, France
[2]Department of Physics, Panjab University, Chandigarh 160 014, India
*Corresponding author. E-mail: amandsood@gmail.com

Abstract. We simulated the central reactions of nearly symmetric and asymmetric systems, for energies at which maximum production of intermediate mass fragments (IMFs) occurred ($E_{\text{c.m.}}^{\text{peak}}$). This study was carried out using hard EOS along with Cugnon cross-section employing MSTB method for clusterization. We studied the various properties of fragments. The stability of fragments was checked through persistence coefficient and gain term. The information about the thermalization and stopping in heavy-ion collisions was obtained via relative momentum, anisotropy ratio and rapidity distribution. We found that for a complete stopping of incoming nuclei very heavy systems are required. The mass dependence of various quantities (such as average and maximum central density, collision dynamics as well as the time zone for hot and dense nuclear matter) was also presented. In all cases (i.e., average and maximum central density, collision dynamics as well as the time zone for hot and dense nuclear matter) a power-law dependence was obtained.

Keywords. Quantum molecular dynamics; intermediate mass fragments; thermalization.

PACS Nos 24.10.Cn; 24.10.Lx

1. Introduction

The heavy-ion collisions at intermediate energies are excellent for studying the nuclear matter at high density and temperature. At high excitation energies, the colliding nuclei compress each other and heat the matter [1–3]. This leads to the destruction of initial correlations, which in turn makes the matter homogeneous and one can have global stopping. The global stopping is defined as the randomization of one-body momentum space or memory loss of the incoming momentum. The degree of stopping, however, may vary drastically with incident energies, mass of the colliding nuclei and colliding geometry. The degree of stopping has also been linked with the thermalization (equilibrium) in heavy-ion collisions. More the initial memory of nucleons is lost, better it is stopped.

The fragmentation of the colliding nuclei into several pieces of different sizes is a complex phenomenon. This may be due to the interplay of correlations and fluctuations

emerging in a collision. Several studies have been carried out to check the fragmentation pattern. Fragmentation pattern has been reported to depend on the size of the colliding nuclei, incident energy as well as impact parameter [1,4–6]. Dhawan *et al* [7] studied the degree of stopping reached in intermediate energy heavy-ion collisions. They found that the degree of stopping decreases with increase in impact parameter as well as at very high energies. They suggested that light charged particles (LCPs) ($2 \leq A \leq 4$), can be used as a barometer for studying the stopping in heavy-ion collisions. Lighter fragments mostly originate from mid-rapidity region whereas intermediate mass fragments (IMFs) originate from the surface of colliding nuclei and can be viewed as remnants of the spectator matter. On the other hand, Sood *et al* [8] studied the thermalization achieved in heavy-ion collisions in terms of participant–spectator matter. They found that participant–spectator matter depends crucially on the collision dynamics as well as history of the nucleons and important changes in the momentum space occur due to the binary nucleon–nucleon collisions experienced during the high dense phase. The collisions push the colliding nucleons into mid-rapidity region responsible for the formation of participant matter. This ultimately leads to thermalization in heavy-ion collisions. Vermani *et al* [8] used rapidity distribution of nucleons to characterize the stopping and thermalization of the nuclear matter. They found that nearly full stopping is achieved in heavier systems like ^{197}Au+^{197}Au whereas in lighter systems a larger fraction of particles is concentrated near the target and projectile rapidities, resulting in a broad Gaussian shape. The lighter systems, therefore, exhibit larger transparency effect, i.e., less stopping. Puri *et al* [9] studied the non-equilibrium effects and thermal properties of heavy-ion collisions. They found that the heavier masses are found to be equilibrated more than the lighter systems.

Recently, Sisan *et al* [10] studied the emission of IMFs from the central collisions of nearly symmetric systems using a 4π-array set-up, where they found that the multiplicity of IMFs shows a rise and fall with increase in the beam energy. They observed that $E^{\max}_{\text{c.m.}}$ (the energy at which the maximum production of IMFs occurs) increases linearly with the system mass, whereas a power-law ($\propto A^{\tau}$) dependence was reported for peak multiplicity of IMFs with power factor $\tau = 0.7$. Though percolation calculations reported in that paper failed to explain the data, subsequent calculations using QMD model [11] successfully reproduced the data over the entire mass. One is, therefore, interested to understand how nuclear dynamics behaves at this peak energy, i.e. whether linear increase reported for the multiplicity of fragments remains valid for other observables or not. We plan here to investigate the degree of stopping reached and other related phenomena in heavy-ion reactions at peak centre-of-mass energies. We also check system size dependence of average and maximum central density, collision dynamics as well as the time zone for hot and dense nuclear matter at the peak centre-of-mass energy.

This study is made within the framework of the quantum molecular dynamics model, which is described in detail in refs [1,4,11–18].

2. Results and discussion

For the present study, we simulated the central reactions ($b = 0.0$ fm) of ^{20}Ne+^{20}Ne, ^{40}Ar+^{45}Sc, ^{58}Ni+^{58}Ni, ^{86}Kr+^{93}Nb, ^{129}Xe+^{118}Sn, ^{86}Kr+^{197}Au and ^{197}Au+^{197}Au at

incident energies at which maximal production of intermediate mass fragments (IMFs) occurs. These read approximately 24, 46, 69, 77, 96, 124 and 104 AMeV, respectively for the above-mentioned systems [11]. Note that at lower incident energies, phenomena like fusion, fission and cluster decay are dominant [19]. Here we used hard (labelled as Hard) equation-of-state along with energy-dependent Cugnon cross-section ($\sigma_{nn}^{\text{free}}$) [15]. The reactions are followed till 200 fm/c. The phase-space was clusterized using minimum spanning tree method with binding energy check (MSTB). The MSTB method is an improved version of the normal MST method [16]. First, the simulated phase-space was analysed with MST method and pre-clusters were sorted out. Each of the pre-clusters was then subjected to binding energy check [11,16]:

$$\zeta_i = \frac{1}{N^{\text{f}}} \sum_{i=1}^{N^{\text{f}}} \left[\frac{(\mathbf{p}_i - \mathbf{P}_{N^{\text{f}}}^{\text{c.m.}})^2}{2m_i} + \frac{1}{2} \sum_{j \neq i}^{N^{\text{f}}} V_{ij}(\mathbf{r}_i, \mathbf{r}_j) \right] < E_{\text{bind}}. \tag{1}$$

We took $E_{\text{bind}} = -4.0$ MeV if $N^{\text{f}} \geq 3$ and $E_{\text{bind}} = 0.0$ otherwise. Here N^{f} is the number of nucleons in a fragment and $\mathbf{P}_{N^{\text{f}}}^{\text{c.m.}}$ is the centre-of-mass momentum of the fragment. This is known as minimum spanning tree method with binding energy check (MSTB) [11,16]. Note that nucleons belong to a fragment if inequality (1) is satisfied. The fragments formed with the MSTB method are more reliable and stable at the early stages of the reactions.

One of the important aspects in fragmentation is the stability of fragments as well as surrounding nucleons of a fragment. The change in the nucleon content of fragments between two successive time steps can be quantified with the help of persistence coefficient [17,18].

Let the number of pairs of nucleons in cluster C at time t is $\chi_{\text{C}}(t) = 0.5 * N_{\text{C}}(N_{\text{C}} - 1)$. At Δt time later, it is possible that some of the nucleons belonging to cluster C have left the cluster and are part of another cluster or are set free or others may have entered the cluster. Now, let N_{C_D} be the number of nucleons that have been in cluster C at time t and are at $t + \Delta t$ in cluster D. We define

$$\Phi_{\text{C}}(t + \Delta t) = \sum_{\text{D}} 0.5 * N_{\text{C}_\text{D}}(N_{\text{C}_\text{D}} - 1). \tag{2}$$

Here the sum runs over all fragments D present at time $t + \Delta t$.

The persistence coefficient of cluster C can be defined as [17,18]

$$P_{\text{C}}\left(t + \frac{\Delta t}{2}\right) = \Phi_{\text{C}}(t + \Delta t)/\chi_{\text{C}}(t). \tag{3}$$

The persistence coefficient averaged over an ensemble of fragments is defined as

$$\left\langle P\left(t + \frac{\Delta t}{2}\right)\right\rangle = \frac{1}{N_{\text{f}_t}} \sum_{\text{C}} P_{\text{C}}\left(t + \frac{\Delta t}{2}\right), \tag{4}$$

where N_{f_t} is the number of fragments present at time t in a single simulation. The quantity is then averaged over a large number of QMD simulations. The stability of a fragment between two consecutive time steps can be measured using persistence coefficient. If the fragment does not emit a nucleon between two time steps, the persistence coefficient is one. On the other hand, if fragment disintegrates completely, the persistence coefficient will be zero. If we remove one nucleon from fragment C, the persistence coefficient is $P_C(t + \Delta t/2) = (N_C - 2)/N_C$, i.e., 0.333 for $N_C = 3$ and 0.8 for $N_C = 10$. For example, for mass 10, when one nucleon is emitted we have two entities at later time step consisting of free nucleon and fragment with mass 9. $P_C(t + \Delta t/2)$ is the contribution from all such entities existing at later times. It, then, measures the tendency of the members of a given cluster to remain together. In figure 1, we display the persistence coefficients for various fragments, i.e., light charged particles (LCPs) ($2 \leq A \leq 4$), heavy mass fragments (HMFs) ($10 \leq A \leq 44$) as well as intermediate mass fragments (IMFs) ($5 \leq A \leq 44$). The various lines have been defined in the caption. It is clear from the figure that the saturation value of persistence coefficient is slightly higher for LCPs compared to heavier fragments. One can conclude that the final fragments are formed after 130 fm/c when this coefficient is 0.8. Before that time there is a strong exchange of nucleons between the fragments. The number of medium and intermediate size fragments increases because the largest fragment falls finally into this mass bracket. The persistent coefficient reaches its asymptotic value later due to the interaction between fragments as well as between fragments and free nucleons. Due to this interaction, nucleons are sometimes absorbed or emitted from the fragments. This process changes the details but not the general structure of the fragmentation pattern.

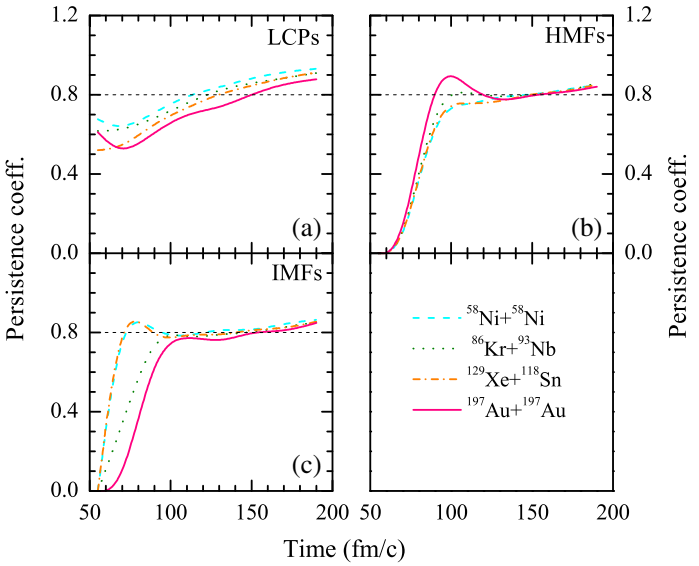

Figure 1. The persistence coefficient as a function of time for LCPs, HMFs and IMFs. Dashed, dotted, dash–dotted and solid lines are for ^{58}Ni+^{58}Ni, ^{86}Kr+^{93}Nb, ^{129}Xe+^{118}Sn and ^{197}Au+^{197}Au, respectively.

Stability of the fragments and thermalization

The persistence coefficient tells about the stability of different fragments between two successive time steps. But it does not provide any information about whether a fragment has swallowed some nucleons or not. To check this, we used a quantity called 'Gain' [18]. The Gain represents the percentage of nucleons that a fragment has swallowed between two consecutive time steps. Let N_α^{f} be the number of nucleons belonging to a fragment α at time t. Let $N_{\alpha\beta}^{\mathrm{f}}$ be the number of nucleons which are in cluster α at time t and are in cluster β at time $t + \Delta t$. The Gain is defined as

$$\mathrm{Gain}(t + \Delta t/2) = \sum_\alpha \eta \times \frac{\sum_\beta (N_\beta^{\mathrm{f}} - N_{\alpha\beta}^{\mathrm{f}})}{N_\alpha^{\mathrm{f}}}. \tag{5}$$

$\eta = 0.0$, 0.5 and 1.0 if $N_{\alpha\beta}^{\mathrm{f}} < 0.5N_\beta^{\mathrm{f}}$, $N_{\alpha\beta}^{\mathrm{f}} = 0.5N_\beta^{\mathrm{f}}$ and $N_{\alpha\beta}^{\mathrm{f}} > 0.5N_\beta^{\mathrm{f}}$, respectively. Naturally, a true Gain for a fragment α is only if its nucleons constitute at least half of the mass of the new fragment β. The Gain will tell us whether the interactions among fragments have ceased to exist or not.

In figure 2, we display the Gain for LCPs, HMFs and IMFs. As discussed earlier, the value of persistence coefficient is slightly higher for LCPs. Therefore, the Gain will be smaller for LCPs as shown in figure 2. It is evident from the figure that for heavier systems the Gain has higher value because of the large nucleon–nucleon interactions.

The quantities which are closely related to the degree of thermalization are relative momentum $\langle K_{\mathrm{R}} \rangle$ and anisotropy ratio $\langle R_{\mathrm{a}} \rangle$. The average relative momentum of two colliding Fermi spheres is defined as [3,9,20]

$$\langle K_{\mathrm{R}} \rangle = \langle |P_P(\mathbf{r}, t) - P_T(\mathbf{r}, t)|/\hbar \rangle, \tag{6}$$

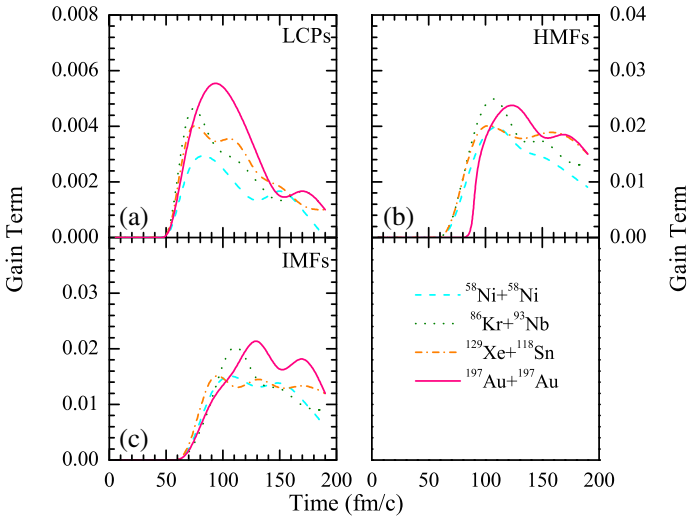

Figure 2. The Gain as a function of time for LCPs, MMFs and IMFs. Lines have the same meaning as in figure 1.

where

$$P_k(\mathbf{r}, t) = \frac{\sum_{j=1}^{A_k} P_j(t)\rho_j(\mathbf{r}, t)}{\rho_k(\mathbf{r}, t)}. \tag{7}$$

Here P_j and ρ_j are the momentum and density experienced by jth particle and k stands for either target or projectile and $\mathbf{r}$ refers to a space point in the central sphere of 2 fm radius to which all calculations are made. The $\langle K_{\mathrm{R}}\rangle$ is an indicator of local equilibrium because it depends on the local position r.

The second quantity is anisotropy ratio which is defined as [3,7,9,20]

$$\langle R_{\mathrm{a}}\rangle = \frac{\sqrt{\langle p_x^2\rangle} + \sqrt{\langle p_y^2\rangle}}{2\sqrt{\langle p_z^2\rangle}}. \tag{8}$$

The anisotropy ratio $\langle R_{\mathrm{a}}\rangle$ is an indicator of global equilibrium of the system because it represents the equilibrium of the whole system and does not depend upon the local positions. The full global equilibrium averaged over a large number of events will correspond to $\langle R_{\mathrm{a}}\rangle = 1$.

In figures 3a and 3b, we display, respectively, $\langle K_{\mathrm{R}}\rangle$ and $\langle R_{\mathrm{a}}\rangle$ ratio as a function of time for different system masses. The initial value of relative momentum increases whereas

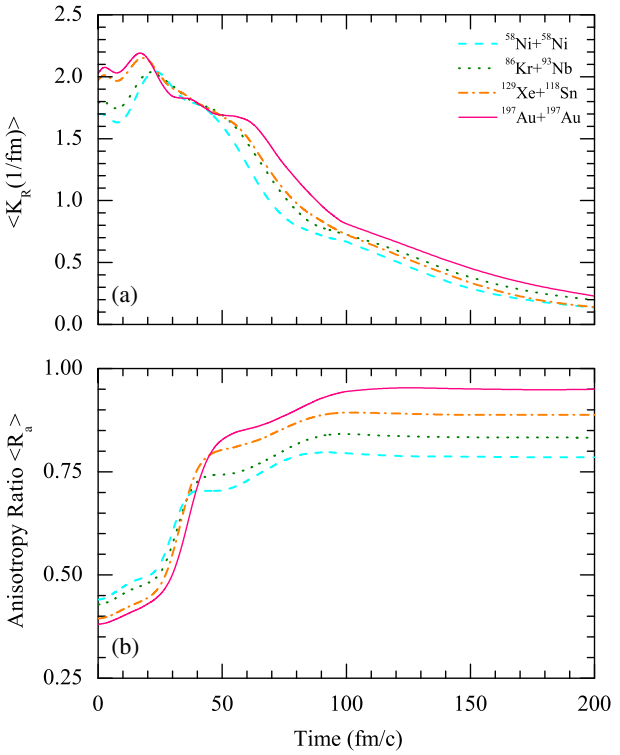

Figure 3. The time evolution of (**a**) relative momentum and (**b**) anisotropy ratio. Lines have the same meaning as in figure 1.

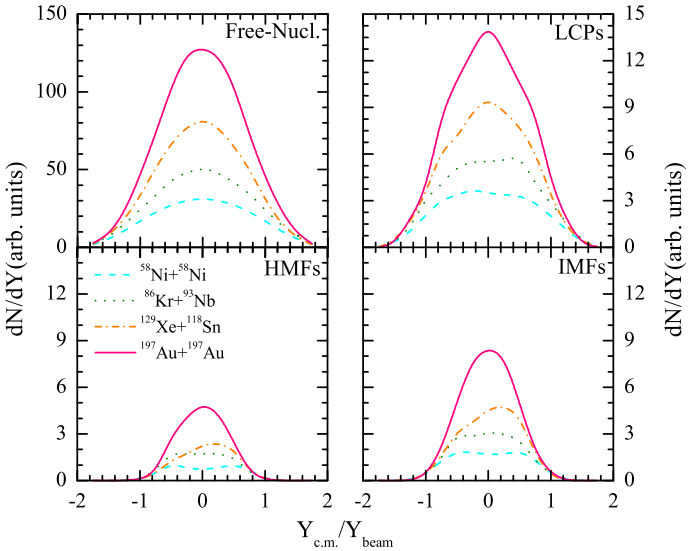

Figure 4. The rapidity distribution, $\mathrm{d}N/\mathrm{d}Y$, as a function of reduced rapidity, $Y_{\mathrm{c.m.}}/Y_{\mathrm{beam}}$. Lines have the same meaning as in figure 1.

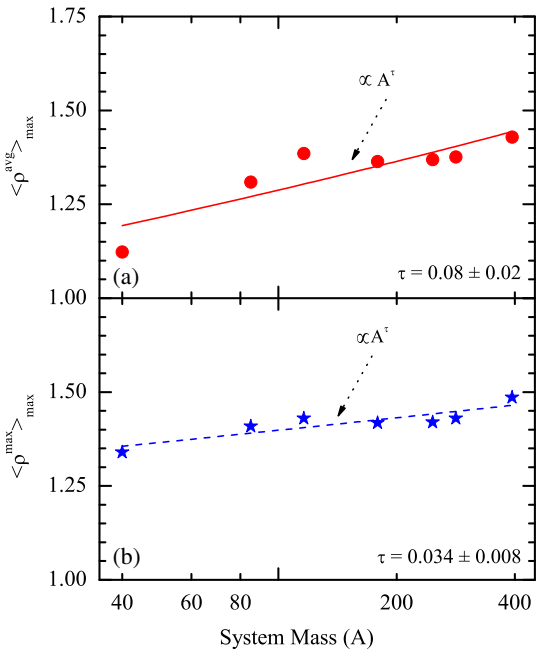

Figure 5. The maximal value of the average density $\langle\rho^{\mathrm{avg}}\rangle_{\mathrm{max}}$ (top) and maximum density $\langle\rho^{\mathrm{max}}\rangle_{\mathrm{max}}$ (bottom) as a function of the composite mass of the system. The solid lines are the fits to the calculated results using A^{τ} obtained with χ^2 minimization. The average is done over all space points on a sphere of 2 fm radius at centre-of-mass.

the anisotropy ratio decreases with mass of the system since $E_{\text{c.m.}}^{\text{peak}}$ increases with increase in the system mass. It is interesting to see that the relative momentum is large at the start of the reaction, and finally at the end of the reaction, the value of $\langle K_{\text{R}} \rangle$ is nearly zero. This means that at the end of the reaction, the local equilibrium is nearly reached. However, the saturation time is nearly the same throughout the mass range. It is clear from figure 3b that the anisotropy ratio changes to a greater extent during the high-density phase. Once the high-density phase is over, no more changes occur in thermalization. Interestingly, heavier nuclei are able to equilibrate more than the lighter nuclei because the number of collisions per nucleon for the ^{197}Au+^{197}Au reaction is larger than that for the ^{58}Ni+^{58}Ni reaction.

The rapidity distribution is also assumed to give information about the degree of thermalization achieved in heavy-ion reactions. The rapidity distribution of the ith particle is defined as [7]

$$Y(i) = \frac{1}{2} \ln \frac{\mathbf{E}(i) + \mathbf{p}_z(i)}{\mathbf{E}(i) - \mathbf{p}_z(i)}. \tag{9}$$

Here $\mathbf{E}(i)$ and $\mathbf{p}_z(i)$ are, respectively, the total energy and longitudinal momentum of the ith particle. Naturally, for a complete equilibrium a single Gaussian shape peak is expected. In figure 4, we display the rapidity distribution of free nucleons, LCPs, HMFs as well as IMFs. Rapidity distribution of all types of fragments indicate that heavier systems are better thermalized compared to lighter ones. For lighter nuclei, we get relatively flat distribution. The effect is more pronounced for different kinds of fragments compared to free nucleons.

In figure 5, we display the system size dependence of the maximal value of average density $\langle \rho^{\text{avg}} \rangle$ (solid circles) and maximum density $\langle \rho^{\text{max}} \rangle$ (solid stars). Lines represent the power-law fitting ($\propto A^{\tau}$). The maximal values of $\langle \rho^{\text{avg}} \rangle$ and $\langle \rho^{\text{max}} \rangle$ follow a power law

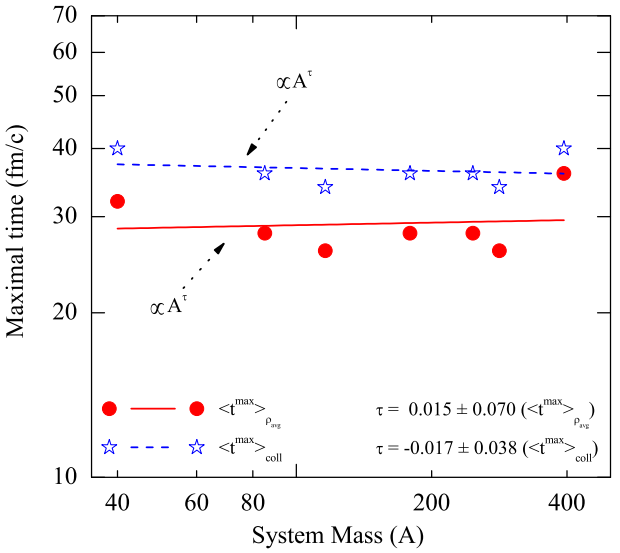

Figure 6. The time of maximal value of collision rate (open stars) and average density (filled circles) as a function of composite mass of the system. The dashed and solid lines represent the χ^2 fits with power law A^{τ}.

($\propto A^{\tau}$) with τ being 0.08±0.02 for the average density $\langle\rho^{\rm avg}\rangle$ and 0.034±0.008 for maximum density $\langle\rho^{\rm max}\rangle$, i.e., a slight increase in density occurs with increase in the size of the system. This is because $E^{\rm peak}_{\rm c.m.}$ increases with the size of the system.

In figure 6, we display the time of maximal collision rate (open stars) and average density $\langle\rho_{\rm avg}\rangle^{\rm max}$ (filled circles) as a function of the total mass of the system. Interestingly, both quantities show a nearly mass-independent behaviour which shows that $E^{\rm peak}_{\rm c.m.}$ increases with the mass of the system in such a way that maximal collision rate and maximal density is achieved at the same time throughout the mass range. The power factor is equal to -0.017 ± 0.038 for maximal time of collision rate and 0.015 ± 0.07 for maximal time of average density.

Apart from the maximal quantities, another interesting quantity is the dense zone at the peak energy. In figure 7, we display the time interval for which $\rho_{\rm avg} \geq \rho_0$ (filled circles) and $\rho_{\rm avg} \geq \rho_0/2$ (open stars). Again, both quantities follow a power-law behaviour with $\tau = 0.15\pm0.05$ and $\tau = -0.04\pm0.06$, respectively, for $\rho_{\rm avg} \geq \rho_0$ and $\rho_{\rm avg} \geq \rho_0/2$. This indicates that the time duration for which $\rho_{\rm avg}$ is greater than the normal nuclear matter density increases with the mass of the system.

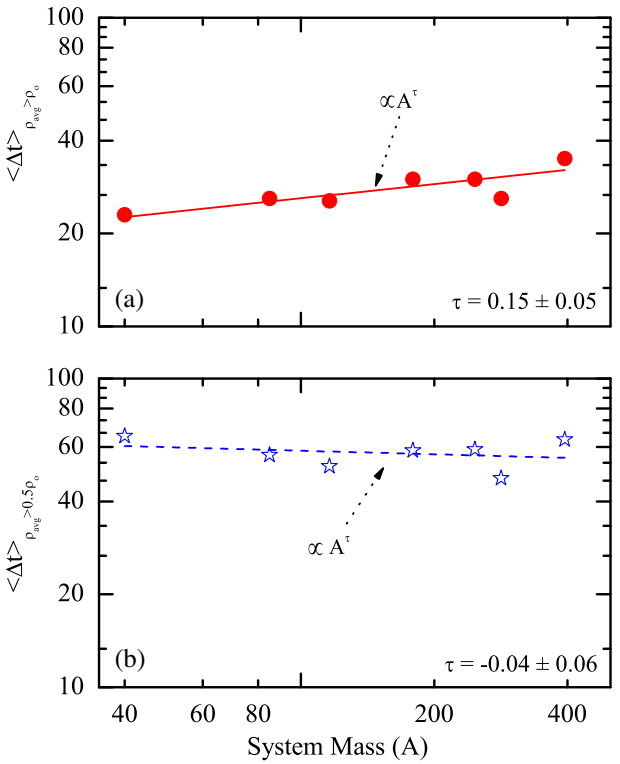

Figure 7. The time zone for $\rho_{\rm avg} \geq \rho_0$ (top) and for $\rho_{\rm max} \geq \rho_0$ (bottom) as a function of composite mass of the system. The solid lines represent the χ^2 fits with power law A^{τ}.

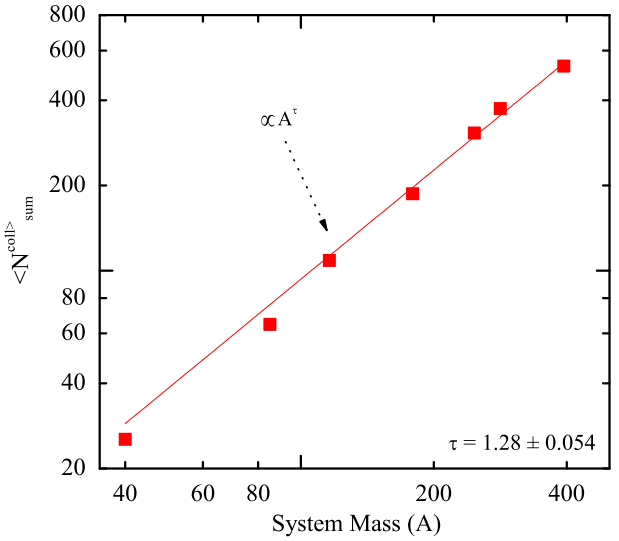

Figure 8. The total number of allowed collisions vs. composite mass of the system. The solid line represents the χ^2 fits with power law A^{τ}.

The system size dependence of the (allowed) nucleon–nucleon collisions (filled squares) is displayed in figure 8. The results are displayed at 200 fm/c where the matter is diluted and well separated. The nucleon–nucleon collisions increase with the system size. This enhancement can be parametrized with a power law proportional to A^{τ} with $\tau = 1.28 \pm 0.054$. At a fixed incident energy, nucleon–nucleon collisions should scale as A. This has been tested by Sood *et al* [21]. Here power factor is greater than one since with increase in mass of the system $E_{\text{c.m.}}^{\text{peak}}$ also increases.

3. Summary

In the present study, we have simulated the central reactions of nearly symmetric and asymmetric systems, for energies at which the maximum production of IMFs occurs ($E_{\text{c.m.}}^{\text{peak}}$), using QMD model. This study was carried out using hard EOS along with Cugnon cross-section and employing MSTB method for clusterization. We have studied various properties of fragments. The stability of fragments is checked using persistence coefficient and Gain. The information about the thermalization and stopping in heavy-ion collisions is obtained via relative momentum, anisotropy ratio and rapidity distribution. We found that for a complete stopping of incoming nuclei very heavy systems are required. The mass dependence of various quantities (such as average and maximum central density, collision dynamics as well as the time zone for hot and dense nuclear matter) is also presented. In all cases (i.e., average and maximum central density, collision dynamics as well as the time zone for hot and dense nuclear matter) a power-law dependence is obtained.

References

[1] P B Gossiaux and J Aichelin, *Phys. Rev.* **C56**, 2109 (1997)
[2] D Hahn and H Stöcker, *Nucl. Phys.* **A476**, 718 (1988)
R K Puri *et al*, *Nucl. Phys.* **A575**, 733 (1994)
Y K Vermani and R K Puri, *Nucl. Phys.* **A847**, 243 (2010)
[3] D T Khoa *et al*, *Nucl. Phys.* **A548**, 102 (1992)
[4] J Aichelin, *Phys. Rep.* **202**, 233 (1991)
[5] M B Tsang *et al*, *Phys. Rev. Lett.* **71**, 1502 (1993)
[6] C Williams *et al*, *Phys. Rev.* **C55**, R2132 (1997)
[7] J K Dhawan *et al*, *Phys. Rev.* **C74**, 057901 (2006)
[8] A D Sood *et al*, *Int. J. Mod. Phys.* **E15**, 899 (2006)
Y K Vermani *et al*, *Phys. Rev.* **C79**, 064613 (2009)
[9] R K Puri *et al*, *J. Phys. G: Nucl. Part. Phys.* **20**, 1817 (1994)
[10] D Sisan *et al*, *Phys. Rev.* **C63**, 027602 (2001)
[11] Y K Vermani *et al*, *J. Phys. G: Nucl. Part. Phys.* **36**, 105103 (2009)
S Kaur and A D Sood, *Phys. Rev.* **C82**, 054611 (2010)
[12] C Hartnack *et al*, *Eur. Phys. J.* **A1**, 151 (1998)
S W Huang *et al*, *Phys. Lett.* **B298**, 41 (1993)
Y K Vermani and R K Puri, *Europhys. Lett.* **85**, 62001 (2009)
Y K Vermani *et al*, *J. Phys. G: Nucl. Part. Phys.* **37**, 015105 (2010)
S Kumar *et al*, *Phys. Rev.* **C78**, 064602 (2008)
[13] S Kumar *et al*, *Phys. Rev.* **C58**, 3494 (1998)
E Lehmann *et al*, *Z. Phys.* **A355**, 55 (1996)
A D Sood *et al*, *Phys. Rev.* **C79**, 064618 (2009)
S Kumar *et al*, *Phys. Rev.* **C81**, 014611 (2010); *ibid*. **81**, 014601 (2010)
E Lehmann *et al*, *Prog. Part. Nucl. Phys.* **30**, 219 (1993)
E Lehmann *et al*, *Phys. Rev.* **C51**, 2113 (1995)
[14] J Singh *et al*, *Phys. Rev.* **C62**, 044617 (2000)
G Batko *et al*, *J. Phys. G: Nucl. Part. Phys.* **20**, 461 (1994)
S W Huang *et al*, *Prog. Part. Nucl. Phys.* **30**, 105 (1993)
C Fuchs *et al*, *J. Phys. G: Nucl. Part. Phys.* **22**, 131 (1996)
A D Sood *et al*, *Phys. Lett.* **B594**, 260 (2004); *ibid*. *Phys. Rev.* **C73**, 067602 (2006)
S Gautam *et al*, *J. Phys. G: Nucl. Part. Phys.* **37**, 085102 (2010)
[15] S Kumar *et al*, *Phys. Rev.* **C58**, 1618 (1998)
R Chugh and R K Puri, *Phys. Rev.* **C82**, 014603 (2010)
[16] J Singh *et al*, *J. Phys. G: Nucl. Part. Phys.* **27**, 2091 (2001)
S Kumar *et al*, *Phys. Rev.* **C58**, 2858 (1998)
[17] R K Puri and J Aichelin, *J. Comp. Phys.* **162**, 245 (2000)
R K Puri *et al*, *Phys. Rev.* **C54**, R28 (1996)
P B Gossiaux *et al*, *Nucl. Phys.* **A619**, 379 (1997)
[18] R K Puri *et al*, *Pramana – J. Phys.* **59**, 19 (2002)
[19] I Dutt *et al*, *Phys. Rev.* **C81**, 047601 (2010); *ibid*. **81**, 044615 (2010); *ibid*. **81**, 064609 (2010); *ibid*. **81**, 064608 (2010)
R Arora *et al*, *Eur. Phys. J.* **A8**, 103 (2000)
R K Puri *et al*, *Phys. Rev.* **C43**, 315 (1991); *ibid*. **45**, 1837 (1992); *ibid*. *J. Phys. G: Nucl. Part Phys.* **18**, 903 (1992); *ibid*. *Eur. Phys. J.* **A3**, 277 (1998); *ibid*. *Eur. Phys. J.* **A23**, 429 (2005)
[20] D T Khoa *et al*, *Nucl. Phys.* **A529**, 363 (1991)
[21] A D Sood *et al*, *Phys. Rev.* **C70**, 034611 (2004)